High Sensitivity Techniques for GNSS Signal Acquisition

1

High Sensitivity Techniques for GNSS Signal Acquisition

Fabio Dovis[1] and Tung Hai Ta[2]
[1]*Politecnico di Torino*
[2]*Hanoi University of Science and Technology*
[1]*Italy*
[2]*Vietnam*

1. Introduction

The requirements of location based and emergency caller localization services spurred by the E-911 mandate (USA) and the E-112 initiative (EU) have generated the demand for the availability of Global Navigation Satellite Systems (GNSS) in harsh environments like indoors, urban canyons or forests where low power signals dominate. This fact has pushed the development of High Sensitivity (HS) receivers

To produce positioning and timing information, a conventional GNSS receiver must go through three main stages: code synchronization; navigation data demodulation; and Position, Velocity and Time (PVT) computation. Code synchronization is in charge of determining the satellites in view, estimating the transmission code epoch and Doppler shift. This stage is usually divided into code acquisition and tracking. The former reduces the code epoch and Doppler shift uncertainties to limited intervals while the latter performs continuous fine delay estimation. In particular, code acquisition can be very critical because it is the first operation performed by the receiver. This is the reason for lots of endeavors having been invested to improve the robustness of the acquisition process toward the HS objective.

Basically, the extension of the coherent integration time is the optimal strategy for improving the acquisition sensitivity in a processing gain sense. However, there are several limitations to the extension of the coherent integration time T_{int}. The presence of data-bit transitions, as the 50bps in the present GPS Coarse-Acquisition (C/A) service, modulating the ranging code is the most impacting. In fact, each transition introduces a sign reversal in successive correlation blocks, such that their coherent accumulation leads to the potential loss of the correlation peak. Therefore, the availability of an external-aiding source is crucial to extend T_{int} to be larger than the data bit duration T_b (e.g. for GPS L1 C/A, $T_b = 20$ ms). This approach is referred as the aided (or assisted) signal acquisition, and it is a part of the Assisted GNSS (A-GNSS) positioning method defined by different standardization bodies (3GPP, 2008a;b; OMA, 2007).

However, without any external-aiding source, the acquisition stage can use the techniques so-called post-correlation combination to improve its sensitivity. In general, there are 3 post-correlation combination techniques, namely: coherent, non-coherent and differential

combination. In fact, the coherent combination technique is equivalent to the T_{int} extension with the advantage that in this stand-alone scenario $T_{int} \leq T_b$. The squaring loss (Choi et al., 2002) caused by the non-coherent combination makes this technique less competitive than the others. However, its simplicity and moderate complexity make it suitable for conventional GNSS receivers. Among the three techniques, the differential combination can be considered as a solution trading-off sensitivity and complexity of an acquisition stage (Schmid & Neubauer, 2004; Zarrabizadeh & Sousa, 1997). As an expanded view of the conventional differential combination technique, generalized differential combination is introduced for further sensitivity improvement (Corazza & Pedone, 2007; Shanmugam et al., 2007; Ta et al., 2012).

In addition, modern GNSSes broadcast new civil signals on different frequency bands. Moreover, these new signals are composed of two channels, namely data and pilot (data-less) channels (e.g. Galileo E1 OS, E5, E6; GPS L5, L2C, L1C). These facts yield another approach, usually named *channel combining acquisition* (Gernot et al., 2008; Mattos, 2005; Ta et al., 2010) able to fully exploit the potential of modern navigation signals for sake of sensitivity improvement.

This book chapter strives to identify the issues related to HS signal acquisition and also to introduce in details possible approaches to solve such problems. The remainder of the chapter is organized as follows. Section 2 presents fundamentals of signal acquisition including the common representation of the received signal, the conventional acquisition process. Furthermore, definition of the the performance parameters, in terms of detection probabilities and mean acquisition time are provided. HS acquisition issues and general solutions, namely stand-alone, external-aiding and channel combining approaches, are introduced in Section 3. In Section 4, the stand-alone generalized differential combination technique is presented together with its application to GPS L2C signal in order to show the advantages of such a technique. Section 5 focuses on introducing a test-bed architecture as an example of the external-aiding signal acquisition. The channel combining approach via joint data/pilot signal acquisition strategies for Galileo E1 OS signal is introduced in Section 6. Eventually, some concluding remarks are drawn.

2. Fundamentals of signal acquisition

2.1 Received signal representation

The received signal after the Analog to Digital Converter in a Direct Sequence Code Division Multiple Access (DS-CDMA) GNSS system can be represented as

$$r[n] = \sqrt{2C}d[n]c[n+\tau]\cos(2\pi(f_{IF}+f_D)nT_S+\varphi)+n_W[n] \quad (1)$$

where C is the carrier power (W); $d[n]$ is the navigation data; $c[n]$ is the spreading code, f_{IF}, f_D denote the Intermediate Frequency (IF) and Doppler shift (Hz) respectively; $T_S = 1/F_S$ stands for the sampling period (s) (F_S is the sampling frequency (Hz)); φ is the initial carrier phase (rad); τ is the initial code delay (samples) ; and n_W is the Additive White Gaussian Noise (AWGN) with zero mean ($\mu = 0$) and variance σ_n^2 ($n_W \sim \mathcal{N}(0, \sigma_n^2)$).

In fact, most of the current and foreseen signals of GNSSes use either BPSK or BOC modulations (Ta, 2010). For these modulations, $c[n]$ has the representation as follows:

- BPSK(f_c):

$$c(t) = \sum_{k=-\infty}^{+\infty} q_k \Pi(t - kT_c) \tag{2}$$

where Π is the rectangular function; q_k is the PRN code. Because of the properties of the PRN code, q_k is a periodic sequence with the period N chips, q_k can be rewriten as $q_k = q_{mod(k,N)}$, then the digital version of (2) is

$$c[n] = c(nT_S) = \sum_{k=-\infty}^{+\infty} q_{mod(k,N)} \Pi\left(nT_S - kT_c\right) \tag{3}$$

being T_c, and $f_c = 1/T_c$ the chip duration (s) and chipping rate (chip per second - cps) respectively.

- BOC(f_s, f_c): Similarly,

$$c[n] = \sum_{k=-\infty}^{\infty} q_{mod(k,N)} s_{mod(k,a/2)} \Pi\left(n - kT_c\right) \tag{4}$$

with $s_{mod(k,a/2)} \in \{-1, 1\}$is the sub-carrier with the frequency f_s and $a = 2\frac{f_s}{f_c}$. Usually in GNSS f_s is a multiple of f_c (i.e. $a/2$ is an integer value) and both the values of f_c and f_s are normalized by 1.023 MHz; for instance BPSK(5) and BOC(10,5) mean $f_c = 5 \times 1.023$ MHz and $f_s = 10 \times 1.023$ MHz. The subcarrier $s[n]$ can be sine-phased, $s[n] = \text{sgn}[\sin(2\pi f_s n T_S)]$; or cosine-phased, $s[n] = \text{sgn}[\cos(2\pi f_s n T_S)]$ with $\text{sgn}(x)$ being the signum function of x.

2.2 Conventional acquisition process

As introduced in (Kaplan, 2005), the conventional acquisition process (see Fig. 1) strives to determine the presence of a desired signal defined by PRN code (c), code delay (τ) and Doppler offset (f_D) in the incoming signal. The uncertainty regions of (c, τ, f_D) form a signal search-space, each cell $(\hat{c}, \hat{\tau}, \hat{f}_D)$ of which is used to locally generate an equivalent tentative signal, see Fig. 2(a). The acquisition process correlates the incoming signal ($r[n]$) with the tentative signal ($\hat{r}[n]$) to measure the similarity between the two signals.

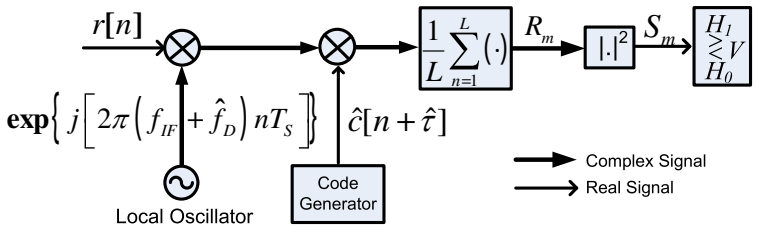

Fig. 1. Conventional signal acquisition architecture

It is well known that there are several general approaches to code acquisition of a GNSS signals. The basic functional operation is a correlation between a local replica of the code and the incoming signal as depicted in Fig. 1, where a serial approach scheme is reported. Time

(or frequency) parallel acquisition approaches, are often efficiently implemented by using Fast Fourier Transform algorithms (Tsui, 2005).

In general, the complex-valued correlation R, which is also referred as Cross Ambiguity Function (CAF), between the incoming and the local generated signals is:

$$\begin{aligned} R_m &= \frac{1}{L}\sum_{n=(m-1)L}^{mL}\{r[n]\widehat{c}[n+\widehat{\tau}]e^{j(2\pi(f_{IF}+\widehat{f}_{D_m}))nT_S}\} \\ &\triangleq s_m + w_m \end{aligned} \tag{5}$$

where m stands for the index of the coherent integration interval $[(m-1)L, mL]$, $\lfloor L = T_{int}F_s \rfloor$ denotes the coherent integration time T_{int} (s) in samples; s_m, w_m are the signal and the noise components respectively, and (Holmes, 2007)

$$\begin{cases} s_m = \sqrt{2C}\mathcal{R}[\theta]\text{sinc}(\triangle\overline{f}_{d_m}T_{int})e^{j(\pi\triangle\overline{f}_{d_k}T_{int}+\phi_m)} \triangleq G_m e^{j\Phi_m} \\ w_m = \frac{1}{L}\sum_{n=(m-1)L}^{mL} n_W[n]\widehat{c}[n+\hat{\tau}]e^{j[2\pi(f_{IF}+\hat{f}_{D_m})nT_S]} \end{cases} \tag{6}$$

where $\theta = \tau - \widehat{\tau}$ is the difference between actual and estimated code delays and $\triangle\overline{f}_{d_m} = f_D - \widehat{f}_{D_m}$ is the difference between Doppler shifts during the interval m, as depicted in Fig. 2(a). ($\phi_m = 2\pi\triangle\overline{f}_{d_{m-1}}T_{int} + \phi_{m-1}$) is the phase mismatch at the end of the m-th interval, and $\mathcal{R}[\theta]$ is the cross-correlation function between the incoming signal and the local PRN codes. In an ideal, noiseless case, such cross-corelation would results to be the autocorrelation function of the two PRNs that can be written for a BPSK signal as

$$\mathcal{R}[\theta] = -\frac{1}{L} + \frac{L+1}{L}\Lambda_0\left(\frac{\theta}{\lambda}\right) \otimes \sum_{m=-\infty}^{\infty}\delta[\theta + mL] \tag{7}$$

and for a BOC signal as (Betz, 2001):

$$\begin{aligned} \mathcal{R}[\theta] = &\left[\Lambda_0\left(\frac{\theta}{\frac{\lambda}{a}}\right) + \sum_{l=1}^{a-1}(-1)^{|l|}\frac{a-|l|}{a}\Lambda_{l\frac{\lambda}{a}}\left(\frac{\theta}{\frac{\lambda}{2}}\right) + \sum_{l=-(a-1)}^{-1}(-1)^{|l|}\frac{a-|l|}{a}\Lambda_{l\frac{\lambda}{a}}\left(\frac{\theta}{\frac{\lambda}{2}}\right)\right] \\ &\otimes \sum_{m=-\infty}^{\infty}\delta[\theta + mL] \end{aligned} \tag{8}$$

where λ is the samples per chip, and Λ is the triangle function of x, centered at z, with a base width of y

$$\Lambda_z\left(\frac{x}{y}\right) = \begin{cases} \left(1 - \frac{|x|}{y}\right) & z \le |x| \le z + y - 1 \\ 0 & \text{elsewhere} \end{cases} \tag{9}$$

From (7) and (8), it can be noted that, when observed over the interval $[-T_c, T_c]$ around the main peak, the autocorrelation function of BPSK signal has the main peak only, whilst the BOC has $(2a-1)$ peaks. Fig. 2(b) shows the theoretical autocorrelation functions of a BPSK(1) and a BOC(1,1). As seen from Fig. 2(b) and Fig. 2(c), the estimation residuals $(\theta, \triangle f_d)$ cause correlation loss on both dimensions. To limit this loss, the cell size $(\triangle\tau, \triangle f_D)$ must be chosen carefully taking into account also the pull-in range of the tracking stage. In general, for BPSK

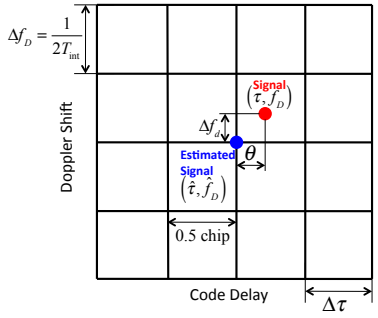

(a)

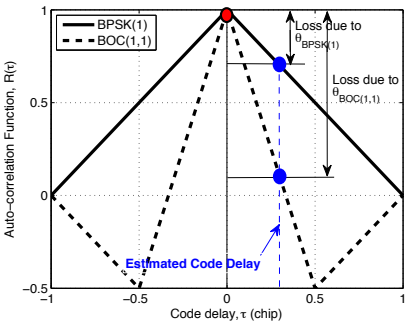

(b)

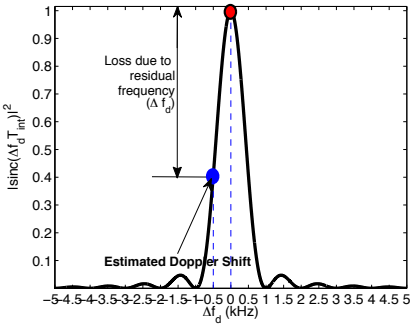

(c)

Fig. 2. (a) Acquisition search-space; (b) Auto-correlation functions of BPSK(1) and BOC(1,1); (c) Sinc function

signal $\triangle\tau_{BPSK} = 0.5$ chip. However, for BOC signal, due to the appearance of side-peaks, $\triangle\tau$ is chosen so that the tracking stage can avoid to lock to the side-peaks. For BOC(1,1), in order to achieve the same average correlation loss as for a BPSK signal, $\triangle\tau_{BOC(1,1)} = 0.16$ chip (Wilde et al., 2006). As for Doppler shift dimension, $\triangle f_D = \frac{2}{3T_{int}}$ as in (Kaplan, 2005) or $\triangle f_D = \frac{1}{2T_{int}}$ as in (Misra & Enge, 2006) are often chosen concerning the trade-off between complexity and sensitivity.

2.3 Acquisition performance parameters

When dealing with real signals, the incoming code is affected by several factors such as propagation distortion and noise, thus resulting in a distorted correlation function. In order to achieve an optimal detection process, the Neyman-Pearson likelihood criterion is used. In fact, the magnitude $S_m = |R_m|^2$ of each complex correlator output can be modeled as a random variable with statistical features. Thus, S_m is compared with a predetermined threshold (V) in order to decide which hypothesis between H_0 ($S_m < V$) and H_1 ($S_m > V$) is true, where H_0 and H_1 respectively represent the absence or presence of the desired peak. Once the decision

is taken, the parameters $\hat{f}_D, \hat{\tau}$ are taken. Such values must belong to the pull-in range of the tracking stage of the receiver.

2.3.1 Statistical characterization of the detection process

As previously remarked, the signal acquisition can be seen as a statistical process, and the value taken by the correlator output for each bin of the search space can be modeled as a random variable both when the peak is absent (i.e. H_0) or present (i.e. H_1). In each case the random variable is characterized by a probability density function (pdf). Fig. 3(a) shows the signal trial hypothesis test decision when both pdfs are drawn. The threshold

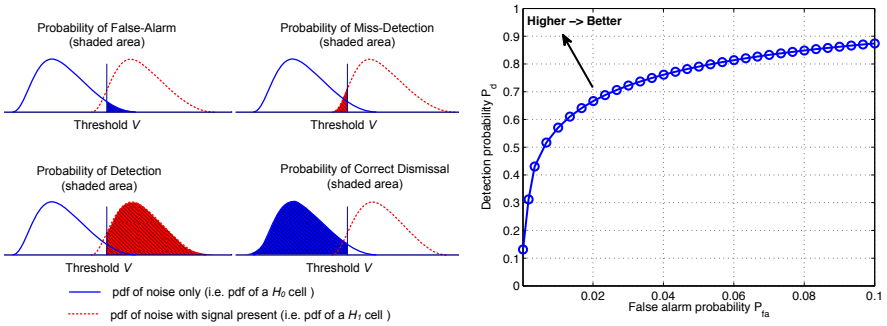

Fig. 3. (a) Possible pdfs of a hypothesis test; (b) Receive Operating Characteristic (ROC) curve

V is pre-determined based on the requirements of: (i) false-alarm probability (P_{fa}), e.g. $P_{fa} = 10^{-3}$, or (ii) mean acquisition time ($\overline{T}_A$), e.g. $\overline{T}_A$ is minimum.

For a specific value of V, there are four possible outcomes as shown in Fig. 3(a). Each outcome is associated with a probability which can be computed by an appropriate integration as (Kaplan, 2005):

- Probability of false-alarm (P_{fa}):

$$P_{fa} = \int_V^{+\infty} f(s|H_0)ds \tag{10}$$

- Probability of correct dismissal (P_{cd}):

$$P_{cd} = 1 - P_{fa} \tag{11}$$

- Probability of detection (P_d):

$$P_d = \int_V^{+\infty} f(s|H_1)ds \tag{12}$$

- Probability of miss-detection (P_{md}):

$$P_{md} = 1 - P_d \tag{13}$$

As described, once P_{fa} and P_d are known, the others can be easily computed. These two probabilities are also used to plot the Receiver Operational Characteristic (ROC) curve (see Fig. 3(b)) depicting the behaviors of the P_{fa} versus P_d for different values of V. This curve is useful for performance comparison among different acquisition strategies.

2.3.2 Peak-to-floor ratios

Theoretical assessment of acquisition performance is not always possible, since it requires also the knowledge of the pdf of the decision variables. For such a reason Monte-Carlo simulation are often employed. In such a case, in order to have suitable confidence in the results, each simulated value of the ROC curve (as in in Fig. 3(b)) has to be the result of the average of million of simulated cases. Therefore, if the sensitivity of a single acquisition scheme in different conditions has to be assessed, it is also useful to consider easy-to-compute parameters, named peak-to-floor ratios, ($\alpha_{max}, \alpha_{mean}$). They are defined as:

$$\alpha_{max} = \frac{\left|S_{peak}\right|^2}{\max\left|S_{floor}\right|^2}; \quad \alpha_{mean} = \frac{\left|S_{peak}\right|^2}{E\left[\left|S_{floor}\right|^2\right]} \tag{14}$$

where S_{peak} is the maximum of the CAF magnitude and S_{floor} is the floor of the CAF magnitude (i.e outside the main correlation peak which is 2 chips wide). These metrics highlight the overall trend of post-correlation Signal-to-Noise Ratio (SNR), avoiding time-consuming calculations or simulations. Anyhow, it is important to point out that the comparison of different acquisition schemes based on the peak-to-floor ratios may be not fair if their decision variables show different statistical properties (Ta et al., 2008).

2.3.3 Mean acquisition time

Let us consider a search-space with N_c columns and N_f rows as in Fig. 2(a), and denote A as a successful detection of a serial acquisition engine (Fig. 1) after some miss-detections and false-alarms. The mean duration from the beginning of the process to the instant when A happens is named mean acquisition time, and can be written as (Park et al., 2002)

$$\overline{T}_A = (N_c N_f - 1)(T_d + T_{fa} P_{fa})\frac{2 - P_d}{2P_d} + \frac{T_d}{P_d} \tag{15}$$

with T_d and T_{fa} being the dwell time and the penalty time respectively.

Equation (15) shows that $\overline{T}_A$ depends on the values of :

- The false-alarm (P_{fa}) and detection (P_d) probabilities at a single cell.
- The search space size $N_c \times N_f$
- The penalty time T_{fa} and the dwell time T_d. In fact, T_{fa} is represented through T_d and the penalty coefficient k_p, $T_{fa} = k_p T_d$. Obviously, T_d depends on each strategy.

Therefore, $\overline{T}_A$ can be seen as the performance parameter taking into account both the computational complexity and the sensitivity of a strategy.

3. High sensitivity acquisition problems

3.1 Acquisition in harsh environments

The conventional acquisition stage in Fig. 1 is designed to work in open-sky conditions. However, in harsh environments, high sensitivity (HS) acquisition strategies are required. In principle, as a nature of DS-CDMA, the longer the coherent integration time (T_{int}) between the local and the received signals is, the better the de-spreading gain (i.e. signal-to-noise ratio improvement) that can be obtained after the correlation process. However, the presence of unknown data bit transitions limits the value of $T_{int} \leq T_b$ (e.g. $T_{int} \leq 20$ ms as for GPS L1 C/A signal) to avoid the correlation loss. This limitation is only neglected if there is an external-aiding source, which provides the data transition information.

The sensitivity improvement obtained by increasing T_{int} is traded-off with an increased computational complexity. As pointed out in Section 2.2, the size of the Doppler step ($\triangle f_D$) reduces as T_{int} becomes larger and this fact increases the search-space size. Furthermore, the instability of the receiver clock causes difficulties for the acquisition stage, especially if T_{int} is large, because of the carrier and code Doppler effects. Therefore, one should consider the trade-off between the sensitivity improvement and the complexity increase when changing the value of T_{int}.

Considering the availability of external-aiding sources and the trade-off between the sensitivity and the complexity, the HS strategies can be divided into:

- Stand-alone approach (to deal with light harsh environments, e.g. light indoor)
- External-aiding approach (to deal with harsh environments, e.g. indoor).

Modern GNSSes broadcast new civil signals on different frequency bands and the new GNSS signals embed the combination of the data channel and a pilot (data-less) channel, per carrier frequency. Examples are E1 OS, E5, E6 signals of Galileo and L5, L2C, L1C signals of GPS. All these facts make possible another approach designed to provide improved acquisition sensitivity:

- Channel combining acquisition approach.

These three approaches are presented in details in the following.

3.2 Stand-alone approach for light harsh enviroments

Without the availability of external aiding sources, the strategies of this approach use $T_{int} \leq T_b$. The sensitivity obtained at a specific value of T_{int} is improved by combining the correlator outputs in different ways: coherent, non-coherent and differential combining. These techniques are referred as post-correlation combination techniques.

3.2.1 Coherent combination

For each cell $(\hat{c}, \hat{\theta}, \hat{f}_D)$ of the search-space, M correlator outputs $\{R_1, R_2, ..., R_m, ..., R_M\}$ obtained by correlating the incoming and the local signals at length T_{int}, see (5), are

considered. As for the coherent technique, these M samples are combined as

$$S_C = \left| \sum_{m=1}^{M} R_m \right|^2 \tag{16}$$

However, (16) can be rewritten to

$$S_C = \left| \frac{1}{N} \sum_{n=0}^{MN} \{ r[n] \widehat{c}[n + \widehat{\tau}] e^{j(2\pi(f_{IF} + \widehat{f}_{D_M}))nT_S} \} \right|^2 \tag{17}$$

As seen in (17), the true value of the coherent integration time is no longer T_{int} but increases to MT_{int}. Hence, it is fair to state that the coherent combination of $\{R_1, ..., R_M\}$ is equivalent to increase T_{int} to MT_{int}, at the cost of an increased complexity.

3.2.2 Non-coherent combination

Unlike the coherent combination, the non-coherent technique combines the squared-envelops of the correlation values $\{R_1, ..., R_M\}$. The mathematical representation of the decsion variable is then

$$S_N = \sum_{m=1}^{M} |R_m|^2 . \tag{18}$$

By using this technique, the main correlation peak also tends to emerge from the noise floor. However, the noise floor is averaged towards a non-zero value. This value is referred as the squaring loss (Choi et al., 2002) and makes the non-coherent combination less effective than the coherent one. However, the effect is not equivalent to an increasing of T_{int}.

3.2.3 Differential combination

This technique was first introduced in the communication field by (Zarrabizadeh & Sousa, 1997). As far as the satellite navigation field is concerned , (Elders-Boll & Dettmar, 2004; Schmid & Neubauer, 2004) are among the first works using this technique and its variants. The mathematical representation of the conventional differential combination is

$$S_D = \left| \sum_{m=2}^{M} R_m R_{m-1}^* \right|^2 \tag{19}$$

As presented in (19), the complex correlator output R_m is multiplied by the conjugate of the one obtained at the previous integration interval R_{m-1}. Then the obtained function is accumulated and its envelope becomes the ultimate decision variable. The fact that the signal component remains highly correlated between consecutive correlation intervals, while the noise tends to be de-correlated, results in the improvement of the technique with respect to the non-coherent one. In comparison with the coherent combination, this technique obtains less de-spreading gain, but also requires less computational resources because the search-space size is unchanged (Yu et al., 2007). Therefore, this technique can be seen as a trade-off solution concerning the pros and cons of the coherent and the non-coherent combination techniques.

However, this technique might suffer from the combination loss due to the unknown data transitions. Assuming that the chance of changing data bit sign after each data bit period is 50%, then if full code correlation (i.e. $T_{int} = 1$ ms) is used, the average degradation due to data overlay is $20\log(18/19) \approx 0.47$ dB. However, in the Galileo case, this loss is scaled to $20\log(1/2) \approx 6$ dB, because the data bit duration is equal to the code length of 4 ms. This fact causes difficulties in applying the differential technique for Galileo E1 OS receivers.

As an expanded view of the conventional differential combination technique, generalized differential combination techniques are introduced to further improve the sensitivity of the acquisition process. These advanced differential techniques will be discussed in details in Section 4.

3.3 External aiding approach for harsh environments

For this approach, basically, the availability of external aiding sources makes the value of T_{int} able to be larger than T_b (i.e. $T_{int} > T_b$). Therefore, in this scenario, increasing T_{int} (or coherent combination of the correlator outputs) is the most suitable solution to give the best sensitivity improvement to the acquisition stage operating in harsh environments. In literature, this approach is also referred as assistance or assisted approach.

As pointed out in (Djuknic & Richton, 2001), the assisted technique enables HS acquisition, since it provides the signal processing chain with preliminary (but approximate) code-phase / Doppler frequency estimates along with fragments of the navigation message. This allows for wiping off data-bit transitions and for extending the coherent integration time. The concept of data-bit assistance has been also introduced by the 3rd Generation Partnership Project (3GPP) in its technical specifications of the Assisted GNSS (A-GNSS) for UMTS (3GPP, 2008a) and GSM/EDGE (3GPP, 2008b) networks.

In general, with all post correlation processing techniques presented in Section 3.2, sensitivity losses are experienced due to

- the residual Doppler error (including the finite search resolution in frequency and the contribution of the user dynamics)
- the uncertainty on the Local Oscillator (LO) frequency.

These effects impact the observed Radio Frequency (RF) carrier frequency and can be more relevant with long coherent integrations (Chansarkar & Garin, 2000) as the case of the coherent combination in this external aiding approach.

Finally, a trade-off between sensitivity and complexity is always necessary, particularly for mass-market receivers (e.g. embedded in cellular phones) which require real-time processing but low power consumption. Despite the recent improvements in chip-set sizes and speeds, a real-time indoor-grade high-sensitivity receiver for cellular phones does not exist yet. Reduced sampling rates are mandatory to minimize the computational load of the baseband processing as well as the optimization of the assistance information exchange is fundamental in order to minimize the communication load which is likely to be paid by the user, according to the latest trends, such as the Secure User Plane for Location (SUPL) defined by Open Mobile Alliance (OMA), (Mulassano & Dovis, 2010; OMA, 2007).

The mentioned A-GNSS specifications, basically define the procedures for requesting and sending information on user position and assistance data. These are typically of two paradigms:

- Mobile-based: assistance data are provided to the User Equipment (UE), which measures the pseudo-ranges and provides the position estimation to the proper network service.
- Mobile-assisted: the UE measures the pseudoranges and sends them to a location server which performs the positioning and service-related tasks.

In both these two modes, the position estimation may benefit of the knowledge of additional information available to the location server gathered from one or more reference receivers (e.g. differential corrections, precise timing and ephemeris, etc.). In the followings, the challenges of the external aiding approach are discussed. It should be noted that the chosen signal for analyses is GPS L1 C/A.

3.3.1 Navigation data wipe-off

The typical effects of both the data wipe-off and non-removed bit transitions are in Fig. 4(a) and Fig. 4(b) respectively. In the first case, the main correlation peak is easily identified whilst in the other one no peak can be distinguished over the floor. Under the AWGN assumption, in

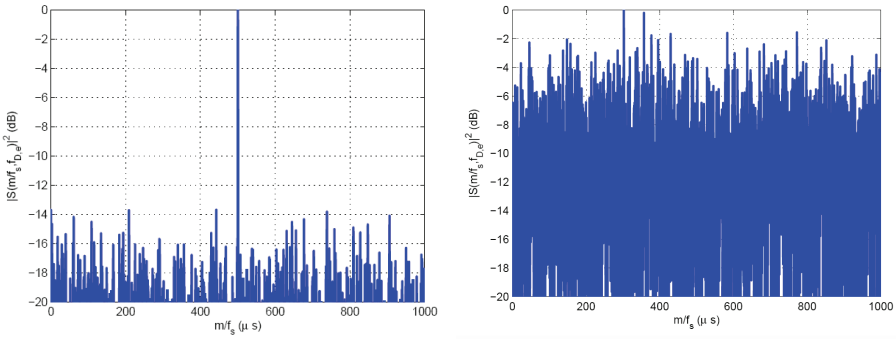

(a) (b)

Fig. 4. CAF along code-phase - simulated GPS L1 C/A signal with code-phase of 500 μs, C/N_0 = 24 dB-Hz and T_{int} = 1 s: (a) with data wipe-off; (b) without data wipe-off

the correct Doppler and code-phase bins α_{mean} is theoretically proportional to post-correlation Signal-to-Noise Ratio (SNR) and it is expected to increase by 3dB when T_{int} doubles. This can be seen in Fig. 5, where we show the effect on α_{mean} and α_{max} of a coherent correlation with $C/N_0 = 24$ dB-Hz and $T_{int} = \{100, 500, 1000\}$ ms performed on simulated GPS signals, both with and without data wipe-off. In Fig. 5(a), we observe that at the highest values of C/N_0 the peak-to-floor ratios change linearly, i.e. α_{mean} increases by 3 dB when T_{int} doubles (e.g. from 500 ms to 1000 ms). In this case, R_{peak} is the correct correlation peak. At the lowest C/N_0, α_{max} is practically 0 dB and the detected peak is likely a noise peak, thus $|R_{peak}|^2 \approx \max |R_{floor}|^2$

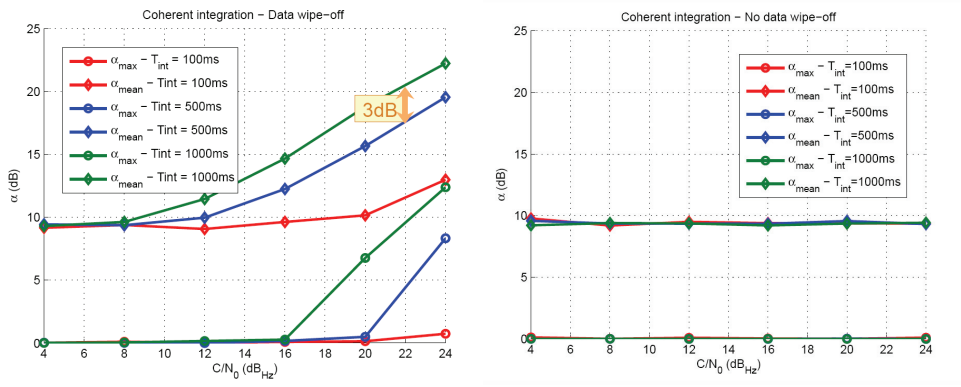

(a) (b)

Fig. 5. α_{mean} and α_{max} vs. C/N_0 and different integration windows: (a) with data wipe-off; (b) without data wipe-off

. α_{mean} is constant for low C/N_0 values because at such a noise level, R_{floor} is a zero-mean Gaussian random variable and for most of $R[k,m]$ samples:

$$|R_{floor}|^2 \leq E\{|R_{floor}|^2\} + \eta\sqrt{Var\{|R_{floor}|^2\}} \tag{20}$$

where η is an arbitrary constant. Then:

$$\alpha_{mean} = \frac{\max\{|R_{floor}|^2\}}{E\{|R_{floor}|^2\}} = 1 + \eta\frac{\sqrt{Var\{|R_{floor}|^2\}}}{E\{|R_{floor}|^2\}} \tag{21}$$

Since R_{floor} is complex and Gaussian distributed, then $|R_{floor}|^2 = \mathcal{R}\{R_{floor}\} + \mathcal{I}\{R_{floor}\}$ is χ^2 distributed (2 degrees of freedom) and thus the ratio of mean and variance is constant (Kreiszig, 1999). In Fig. 5(b), it can be seen that without data wipe-off the CAF envelope behaves as if it is made of noise only, even at the highest values of C/N_0.

3.3.2 Doppler effects on carrier and code

The Doppler effect observed at the receiver location is caused by the time-variant propagation delay of the transmitted signal along its path toward the receiver. This delay changes over time even in case of a low-dynamics user (e.g. pedestrians, etc.), as at least the SV is moving along its own orbit. Even if the rate of change is relatively slow, when long coherent integration windows are used, it can be shown that it impacts on the acquisition sensitivity. Let (22) be the general expression of the received RF signal (noiseless for simplicity):

$$s_{RX}(t) = \sqrt{2C}c[t - \tau(t)]\cos\{2\pi f_{RF}[t - \tau(t)]\} \tag{22}$$

where $\tau(t)$ is the time-variant propagation delay. With a first-order expansion of the time-variant delay, i.e. $\tau(t) = \tau_0 + a \cdot t + ...$, the carrier phase becomse:

$$\begin{aligned} 2\pi f_{RF}[t - \tau(t)] &= 2\pi f_{RF}(t - \tau_0 - a \cdot t) = \\ &= 2\pi f_{RF} t - 2\pi f_{RF}\tau_0 - 2\pi f_{RF} a \cdot t = \\ &= [2\pi(f_{RF} + f_D)t + \varphi_0] = \end{aligned} \tag{23}$$

Let us denote $\varphi_0 = -2\pi f_{RF}\tau_0$ and $f_D = -2\pi f_{RF} a$ then

$$2\pi f_{RF}[t - \tau(t)] = \left[2\pi f_{RF}\left(1 + \frac{f_D}{f_{RF}}\right)t + \varphi_0\right] \tag{24}$$

where $f_D = -a f_{RF} = -f_{RF}\dfrac{d\tau(t)}{dt}$ is the usual Doppler frequency shift. Due to the Doppler effect, the observed carrier frequency is different from the nominal RF carrier frequency. With a second-order expansion for $\tau(t)$, we could see that also f_D changes in time and we could take into account a Doppler-rate term r_D. For a ground GPS receiver in low-dynamics conditions, the typical intervals are $f_D = -5$ kHz $\div 5$ kHz and $r_D = -1$ Hz/s $\div 0$ Hz/s.

The IF down-conversion leaves unmodified the Doppler frequency, as the IF carrier results:

$$BPF\{\cos[2\pi(f_{RF} + f_D)t + \phi_0] \cdot 2\cos[2\pi(f_{RF} - f_{IF})t]\} = \cos[2\pi(f_{IF} + f_D)t + \phi_0 + \phi_{RX}] \tag{25}$$

where BPF $\{\}$ refers to the front-end filtering operation performed by the down-conversion stage and φ_{RX} is the related additional phase contribution.

The code component is theoretically periodic with fundamental frequency equal to the inverse of the code period. When propagating from the satellite to the receiver, the same time-variant delay impacts on all the harmonic components:

$$\begin{aligned} c[t - \tau(t)] &= \sum_{h=0}^{\infty} \mu_h e^{j2h\pi f_0[t-\tau(t)]} \\ &= \sum_{h=0}^{\infty} \mu_h e^{j2h\pi f_0\left(1+\frac{f_D}{f_{RF}}\right)t+\vartheta_0} \end{aligned} \tag{26}$$

Due to the Doppler effect, each harmonic is shifted of the same relative frequency offset $\left(1 + \dfrac{f_D}{f_{RF}}\right)$. Thus the fundamental frequency of the delayed code is now $f_0\left(1 + \dfrac{f_D}{f_{RF}}\right)$ and its period duration is:

$$T_{code} = \frac{\tilde{T}_{code}}{\left(1 + \dfrac{f_D}{f_{RF}}\right)} \tag{27}$$

where $\tilde{T}_{code}$ is the nominal one. Consequently, the true chip rate is

$$R_c = \tilde{R}_c\left(1 + \frac{f_D}{f_{RF}}\right) \tag{28}$$

f_D (kHz)	α_{max} (dB)	α_{mean} (dB)	Doppler-induced code-phase estimation error (chips)
-5	0.01	14.18	1.683
-2.5	2.66	18.88	0.830
0	12.77	22.48	0
2.5	2.22	18.93	-0.839
5	0.19	14.47	-1.838

Table 1. Peak-to-floor ratios and Doppler effect on estimated code phase, $C/N_0 = 24$ dB-Hz and $T_{int} = 1$ s.

During the acquisition phase, if the local code is generated at the nominal chip rate R_c, the correlation between local and received codes suffers a loss due to the difference with the true received chip rate R_c. Furthermore, such a loss increases with the integration times. A loss of about 8 dB in α_{mean} can be estimated at $C/N_0 = 24$ dB-Hz ($T_{int} = 1$ s). Table 1 shows the degradation of the correlation peak and the code-phase estimation error.

3.3.3 Local oscillator stability

The uncertainty on the nominal value f_{LO} of the LO frequency is usually expressed as fractional frequency deviation (Audoin & Guinot, 2001):

$$y_{LO}(t) = \frac{\triangle f(t)}{f_{LO}} = \frac{f(t) - f_{LO}}{f_{LO}} = \frac{f(t)}{f_{LO}} - 1 \tag{29}$$

where $f(t)$ is the true instant frequency. y_{LO} is affected by environmental conditions (e.g. temperature, pressure), dynamic stress (e.g. acceleration, jerk, etc.), circuital tolerances, etc. The time deviation (i.e. the time difference between the clock with the true oscillator and an ideal clock), is given by:

$$x_{LO}(t) = \int_{-\infty}^{t} y_{LO}(u)du \tag{30}$$

With the zero-th order expansion $y_{LO}(t) = y_0 + ...$, (y_0 is a constant frequency offset), the time deviation results:

$$x_{LO}(t) = x_0 + y_0 \cdot t \tag{31}$$

where x_0 is an initial synchronization error between real and ideal clocks and t is the time elapsed since the initial synchronization epoch. This model can be used to evaluate the effect of the local oscillator accuracy on both the down-conversion and the sampling stages.

During the down-conversion the true mixing signal (used in (25)) is:

$$2\cos[2\pi(f_{RF} - f_{IF})(1 + y_0 t)] \tag{32}$$

The true IF carrier is actually affected by an additional unpredictable shift, that prevents the exact carrier frequency estimation, even with very accurate Doppler aiding information. By means of (31) we can evaluate the impact of the LO on the sampling process. With the true

sampling clock, the sampling timescale can be defined as:

$$t_S(s)\Big|_{t=\frac{n}{f_S}} = \frac{n}{f_S} + x_{LO}\left(\frac{n}{f_S}\right) = \frac{n}{f_S} + x_0 + y_0\frac{n}{f_S} \qquad n = 0, 1, 2, ... \tag{33}$$

where n/f_S is the ideal sampling instant and f_S is the sampling frequency. The sampled version of the IF signal is:

$$r[n] = r\left(\frac{n}{f_S} + x_0 + y_0\frac{n}{f_S}\right) \tag{34}$$

and it is affected by a time-variant delay with respect to the ideal case. This gives rise to an equivalent Doppler effect, as previously discussed, and hence to an additional correlation loss. Oscillators typically used in GNSS receivers are mostly Crystal Oscillators (XOs) with some degree of frequency stabilization, e.g. Thermally-Compensated Crystal Oscillator (TCXO), with typical accuracy $y_{LO} \sim 10^{-6}$ and Oven-Controlled Crystal Oscillator (OCXO), with typical accuracy $y_{LO} \sim 10^{-8}$ (Vig, 2005). Table 2 shows how a constant offset on the LO frequency may impact both on α_{mean}, α_{max} and on the accuracy of the code-delay estimation in case of a 1 s coherent integration.

f_D/f_{LO}	$\alpha_{max}(dB)$	α_{mean} (dB)	Code-phase error (chips)
0	22	31	0
$0.5 \cdot 10^{-6}$	18	31	0.75
$1.5 \cdot 10^{-6}$	0	27	1.5

Table 2. Constant offset on LO frequency. $T_{int} = 1$ s, $C/N_0 = +\infty$

3.4 Channel combining approach:

- Channel Combining on Different Carrier Frequencies

In a new or upgraded GNSS, there are several civil signals broadcast in different frequencies. This fact assures a future for civil GNSS dual-frequency receivers, which are now used only in high-value professional or commercial applications such as survey, machine control and guidance, etc. Beside the predictable advantages, such as ionosphere error elimination and carrier phase measurement improvement, civil dual-frequency receivers also offer sensitivity improvement by making possible combined acquisition strategies. The combined acquisition on different carrier frequencies is guaranteed by the fact that the signal channels belonging to a common GNSS are time synchronized, and the Doppler shifts of these channels are related by the ratio among the carrier frequencies. In literature, (Gernot et al., 2008) uses this approach for combined acquisition of GPS L1 C/A and L2C signals.

- Channel Combining on a Common Frequency:

New GNSS signals are composed of data and pilot (data-less) channels. These two channels can be multiplexed by Coherent Adaptive Subcarrier Modulation (e.g. Galileo E1 OS), Time Division Multiplexing (GPS L2C) and Quadrature Phase-Shift Keying (Galileo E5; GPS L5,

L1C). The transmitted power is shared between two channels. Therefore, if the acquisition is performed on both channels, then the better sensitivity improvement can be obtained. In literature, (Mattos, 2005; Ta et al., 2010) use this approach for Galileo E1 OS signal acquisition.

Essentially, for the channel combining acquisition approach (common or different frequencies), in each involved channel, an acquisition strategy belonging to either the stand-alone or the external-aiding approach is performed. Then the acquisition outputs from all the channels are combined in different ways. In Section 6, the joint data/pilot acquisition strategies for Galileo E1 OS signal is introduced as an example for this approach.

4. Stand-alone approach: Generalized differential combination technique

4.1 Technique description

As seen in (19), the decision variable of the Conventional Differential Combination (CDC) technique is an accumulation of the products between two consecutive correlator outputs $R_m,\ R_{m-1}$. In a broader manner, the Generalized Differential Combination (GDC) has been introduced (Corazza & Pedone, 2007; Shanmugam et al., 2007). This technique considers the products of two consecutive correlator outputs as in CDC as well as the products of two correlator outputs at all sample distances or referred as all possible spans, see Fig. 6(a). Let us

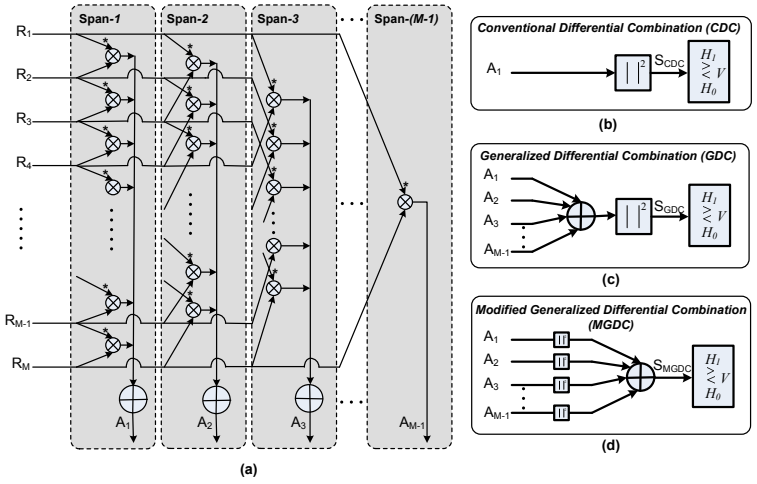

Fig. 6. Differential Post Correlation Processing Architecture: (a) Differential operations; (b) Conventional Differential Combination (CDC); (c) Generalized Differential Combination (GDC); (d) Modified Generalized Differential Combination (MGDC)

define a span-i term as:

$$A_i = \sum_{m=i+1}^{M} R_m R_{m-i}^* \tag{35}$$

Then the decision variable of GDC (Fig. 6(c)) is

$$S_{GDC} \triangleq \left| \sum_{i=1}^{M-1} A_i \right|^2 \tag{36}$$

Note that the CDC technique is in fact the GDC taking into account span-1 A_1 only, see Fig. 6(b). Basically, the GDC technique can be considered as a coherent integration of the differential combinations at different sample distances. Following the analyzes in (Ta et al., 2012), with small M (e.g. $M \leq T_b/T_{int}$), in normal circumstances with normal user dynamic and frequency standards, the average frequency drift is small and tends to zero. Therefore, the values of $G_m, \triangle\bar{f}_{d_m}$ in (6) are constant for all $m \in [0, M-1]$. The signal component A_i^S of an arbitrary span-i (A_i) in (35) can be represented as

$$A^S_{i|\tau,\triangle\bar{f}_d} = \sum_{m=i}^{M} G^2 e^{j2\pi i \triangle\bar{f}_d T_{int}} \tag{37}$$

with

$$\begin{cases} \triangle\bar{f}_d = \triangle\bar{f}_{d_1} = ... = \triangle\bar{f}_{d_M} \\ G = G_1 = ... = G_M = \sqrt{2C}\mathcal{R}[\tau]\text{sinc}(\triangle\bar{f}_d T_{int}) \end{cases} \tag{38}$$

For the GDC technique, substituting (37) into (36), S_{GDC} is computed

$$S_{GDC} = |D|^2 = \left| \sum_{i=1}^{M-1} G^2 e^{j2\pi i \triangle\bar{f}_d T_{int}} \right|^2 \tag{39}$$

Equation (39) shows that the residual carrier phase is still present in the d_{GDC}. This fact causes an unpredictable loss, which depends on the specific value of $\triangle\bar{f}_d$. To eliminate this loss, Modified Generalized Differential Combination (MGDC) technique (Ta et al., 2012) can be used, see Fig. 6(d). Following this technique, the decision variable of the MGDC technique is

$$S_{MGDC} = \sum_{i=1}^{M-1} |A_i|. \tag{40}$$

If the noise is neglected, (40) becomes

$$\begin{aligned} S_{MGDC} = \sum_{i=1}^{M-1} |A_i^S| &= |(M-1)G^2 e^{j2\pi\triangle\bar{f}_d T_{int}}|^2 + |(M-2)G^2 e^{j4\pi\triangle\bar{f}_d T_{int}}|^2 + ... \\ &+ |G^2 e^{j2\pi(M-1)\triangle\bar{f}_d T_{int}}|^2 = (M-1)G^2 + (M-2)G^2 + ... + G^2 = \frac{M(M-1)}{2}G^2 \end{aligned} \tag{41}$$

By forming the decision variable in this way, the unpredictable loss caused by the residual carrier phase is canceled completely. However, the non-coherent integrations between all the spans make the noise averaging process worse than for GDC.

Note: for the GDC and MGDC techniques, the number of spans involved can vary from 1 to $M-1$. By default, all $(M-1)$ possible spans are considered as in (40). If a different number

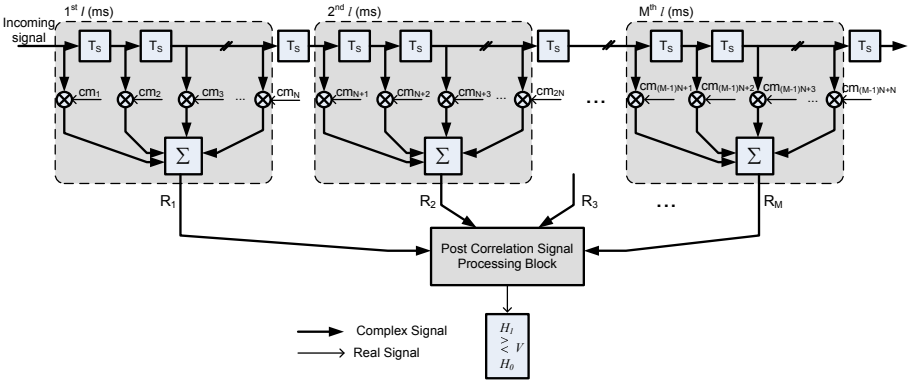

Fig. 7. L2C Partial acquisition using matched filter

of spans i ($1 \leq i \leq M-1$) is used, in the following, the notations for the two techniques will be GDC(i) and MGDC(i).

4.2 Application of technique to L2C signal

In this Section, the MGDC technique is used to acquire GPS L2C signal. This signal is chosen because it employs a long PRN code period, which can be used to generate partial correlator outputs with the same sign. Hence, there is no combination loss due to data bit transitions in differential accumulation (see Section 3.2.3).

4.2.1 L2C signal acquisition

The L2C signal has advantages in interference mitigation due to its advanced PRN code format. This signal is composed of two codes, namely L2 CM and L2 CL. The L2 CM code is 20-ms long containing 10230 chips; while the L2 CL code has a period of 1.5 s with 767250 chips. The CM code is modulo-2 added to data (i.e. it modulates the data) and the resultant sequence of chips is time-multiplexed (TM) with CL code on a chip-by-chip basis. The individual CM and CL codes are clocked at 511.5 kHz while the composite L2C code has a frequency of 1.023 MHz. Code boundaries of CM and CL are aligned and each CL period contains exactly 75 CM periods. This TM L2C sequence modulates the L2 (1227.6 MHz) carrier (GPS-IS, 2006). The original L2C data rate is 25 bps but a half rate convolutional encoder is employed to transmit the data at 50 sps. Consequently, each data symbol matches the CM period of 20 ms.

With these specifications, the common signal representation in (1) is changed to

$$r[n] = \sqrt{2C}\{d[n]c_{\mathrm{m}}[n+\tau] + c_{\mathrm{l}}[n+\tau+kP]\}\cos[2\pi(f_{IF}+f_D)nT_S+\varphi] + n_W[n] \qquad (42)$$

where $c_{\mathrm{m}}[n]$ and $c_{\mathrm{l}}[n]$ are the received CM and CL codes respectively (samples); θ is the received signal delay; P refers to the number of samples in a full CM code period (i.e. 20 ms), $0 \leq k \leq 74$ is an integer that gives the CL code delay relative to CM code.

Fig. 7 shows an architecture of the partial acquisition suitable for L2C CM signal. A segmented matched filter (MF) is used as a correlator (Dodds & Moher, 1995; Persson et al., 2001). The

MF is loaded with one full modified CM code. The modified CM code is obtained from the original CM code with every alternative sample being zero padded to account for the TM structure. The MF does not produce the correlation results equivalent to the full code period, i.e. $T_{int} = 20$ ms. Nevertheless, it provides M partial correlation results with $T_{int} = l$ ms as in Fig. 7. It can be thought of as the partial acquisition process using M different local codes of 1-ms length. By setting the local codes in this way, the signal components of all M correlator outputs $R_1, ..., R_M$ have the same sign. Therefore, the differential combination can be used among these M outputs without any loss from the data transition effect. These M correlator outputs are then directed to Post Correlation Signal Processing Block, which contains 3 differential combination solutions, namely CDC, GDC and MGDC, as presented in Section 4. The analytical expressions of the performance parameters of these techniques can be found in (Ta et al., 2012).

4.2.2 Performance analyses

Summarizing the techniques introduced in the previous sections, there are five strategies that have to be investigated: non-coherent, CDC, GDC, MGDC and 20-ms coherent combination (full code acquisition). Fig. 8 shows the behavior of the detection probabilities of all the strategies when $T_{int} = 1$ ms, $P_{fa} = 10^{-3}$ and the signal strength (C/N_0) varies. The 20-ms coherent technique, as expected, has the best performance. Among the others, all the differential post correlation processing techniques, i.e. GDC, MGDC, CDC, are better than the non-coherent one. The CDC technique taking into account only Span-1 provides the lowest improvement of 1 dB with respect to the non-coherent. The performance of MGDC with different numbers of spans involved (i.e. span size) is also shown in Fig. 8(a). It can be observed that as the span size increases, the detection capability also improves. For the highest span size (i.e. 19 in the figure), the MGDC can offer an advantage of more than 1 dB over the CDC as well as more than 2 dB over the non-coherent combination. These improvements are preserved even the worst case is considered as can be seen in Fig 8(b). Among the differential techniques, the GDC has the highest performance. If all the spans are considered, the GDC performance approaches that of the coherent one. However, this performance is only guaranteed when the residual carrier phase is known (i.e. the perfect case). In Fig. 8(b), the detection probability of the GDC technique reduces dramatically due to the residual carrier phase. Table 3 compares the simulation results of $\overline{T}_A$ for the normal

T_{int} ms	$\overline{T}_A$ ($\times 10^5$) ms	Relative Savings
0.5	0.08527	97.15%
1	0.1624	94.5%
2	0.313	89.5%
5	0.769	74.3%
10	1.519	49.3%
20	2.996	0%

Table 3. Reduction of Mean Acquisition Time by using MGDC at different partial coherent integration times with respect to full 20-ms acquisition ($C/N_0 = 23$ dB-Hz)

outdoor operating range of signal power, i.e. above 32 dB-Hz. It can be observed that a significant saving in $\overline{T}_A$ of MGDC (with respect to the full CM period correlation acquisition) can be achieved by shortening T_{int}.

5. External aiding acquisition technique for indoor positioning

In this section, a test-bed architecture, which is proposed by (Dovis et al., 2010), is introduced as an example of the external-aiding acquisition approach.

5.1 Test-bed architecture

The test-bed as seen in Fig. 9 includes two chains:

Test receiver chain: The main task of this chain is to collect a snapshot of the digitized GPS signal and sends it to a location server through a cellular communication channel. The chain consists of a GPS L1 front-end with the antenna at the test location. The RF front-end is connected to a PC which collects digital sample streams into binary files. The local oscillator is a rubidium (Rb) frequency standard (Datum8040, 1998) running the front-end through a waveform synthesizer (HP, 1990).

Reference receiver chain: The main task of this chain is to perform the HS acquisition process taking advantage of the available assistance information. The chain consists of a reference GPS receiver which processes open-sky signals from a fixed (known) location and provides measurements to an assistance server. The latter provides the necessary aiding information to the HS acquisition engine and the GPS Time indication for the synchronization of the sample-stream recorder, performed before starting each signal collection session. The synchronization process introduces an uncertainty on the GPS Time tags, since it is performed by the software running at the PC, which is assumed to be 2s as in this work.

The assistance server is a software tool developed at Telecom Italia Laboratories to support several test activities on Assisted GPS (A-GPS) technologies. It collects data from the reference receiver and generates time-tagged log files with several kind of assistance information to be provided to the HS acquisition engine. Each line of the log file, for each visible SV, contains code-phase, Doppler frequency and Doppler rate estimates.

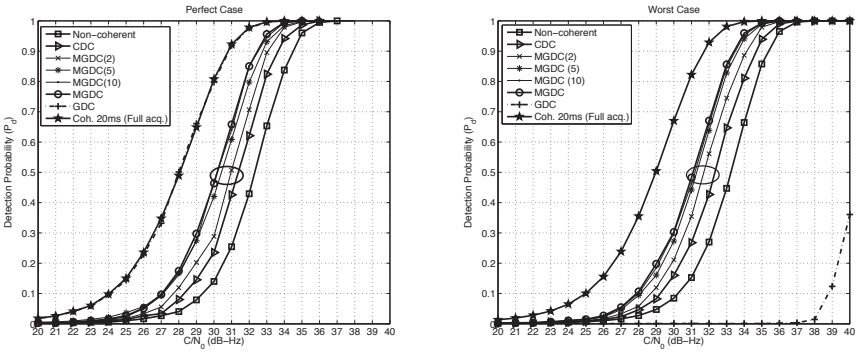

(a) (b)

Fig. 8. Detection probability (P_d) of all post-correlation processing techniques at different signal power levels in (a) perfect case: $\triangle \bar{f}_d = 0$ Hz; (b) worst case: $\triangle \bar{f}_d = 12.5$ Hz for coherent combination (i.e. full 20-ms acquisition) and $\triangle \bar{f}_d = 250$ Hz for the other techniques.

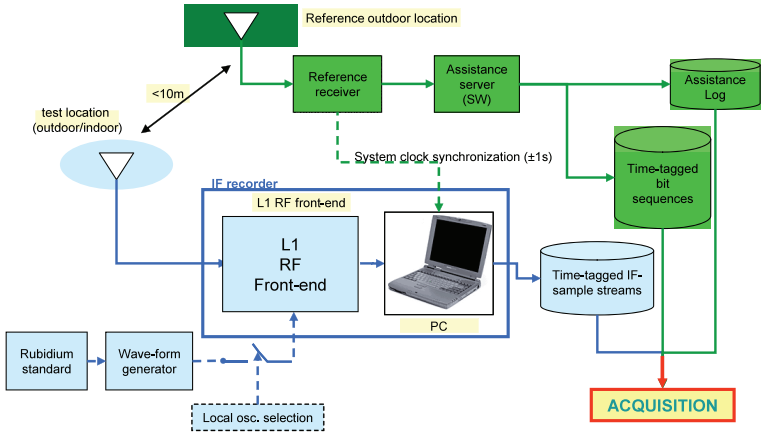

Fig. 9. Test bed architecture: reference chain (green) and test chain (blue)

5.2 Acquisition procedure

- Step 1 - Preliminary fast detection of the strongest PRN

In this step, the FFT-based circular correlation stage is used to quickly detect the best PRN selected on the basis of the predicted C/N_0 and elevation. The value of T_{coh} is 10ms and; the number of M correlator outputs is then non-coherently combined to achieve a sufficient post-correlation SNR; $\triangle f_D$ =100 Hz (trade-off between frequency resolution and search complexity), while the code-phase search space spans over a full code period.

- Step 2 - Determination of the assistance offsets

Code-phase and frequency offsets are caused by: (i) space displacement of test and reference antennas (mostly code-phase offset); (ii) the time offset between the reference receiver and test receiver clocks (code-phase offsets); and (iii) the uncertainty on the test receiver LO frequency (Doppler frequency offset). In this step, these offsets, which are the same for all the PRNs, can be computed by considering the difference of the preliminary estimates (from step 1) with those provided by the assistance data.

- Step 3 - Aided long coherent correlation with data wipe-off on weaker PRNs

The offsets obtained with the strong PRN can be used to correct the assistance predictions and finely determine the code-phase/Doppler frequency of other PRNs at the last step (aided long coherent correlation), ensuring the best achievable post-correlation SNR by means of a low-complexity data wipe-off technique. At this step, the frequency bin size of $\triangle f_{D,3} = 1/T_{coh}$ (e.g. $\triangle f_{D,3} = 1$ Hz if $T_{coh} = 1$ s) is used, over a frequency search space 100 Hz wide (i.e. the residual uncertainty from step 1), and a code-phase search range 6 chips wide. The knowledge of aiding data would allow for a narrower search space, but the acquisition has to account for possible residual errors between the true and predicted code phases.

The code-phase resolution is as low as 1 sample (for both step 1 and 3). The reference signal bandwidth is $B = 2.046$ MHz chosen to match the main lobe (two-sided) of the GPS signal spectrum. Therefore the performed tests have been run with a sampling rate $f_S = 4.092$ MHz

designed to meet the Nyquist criterion. Finally the local code rate taking into account the Doppler effect, as presented in (27), is used.

5.3 Data wipe-off mechanism

In order to increase the coherent integration over the data bit duration (i.e. 20 ms), the acquisition stage performs data wipe-off process. Basically, the conventional data wipe-off process is done as follows

$$R = \frac{1}{N}\sum_{n=1}^{MN} \widehat{d}[n] \cdot \{r[n]\widehat{c}[n+\widehat{\tau}]e^{j(2\pi(f_{IF}+\widehat{f}_D))nT_S}\} \tag{43}$$

with $\{\widehat{d}[n] |\ n = 1...MN\}$ being the data sequence provided by the assisted data. However, at the acquisition stage, the signal snap-shot and the assisted data are not synchronized. Therefore, in order to determine the correct bit sequence for the signal snap-shot, the acquisition stage needs to test all possible data sequence in a predetermined uncertainty. Then the maximum likelihood estimator is used for decision. Hence, it can be said that the acquisition stage in this scenario searches for the presence of a desired signal on 4-dimensions, namely: PRN, code-phase, frequency and bit-phase (i.e. 4D search-space).

In fact, this mechanism requires an unacceptable computational effort for a single position fix, because for each bit-phase (i.e. a data bit sequence candidate), the whole search-space must be re-computed. As a result, the number of elementary steps (i.e. multiply&add) is

$$(T_{coh} \cdot f_S) \times (N_{cp} \cdot N_f) \times N_{bit-seq} = 4.092 \cdot 10^8 \cdot N_{cp} \cdot N_f \tag{44}$$

with N_{cp}, $N_f, N_{bit-seq}$ being the numbers of code-phase, Doppler frequency and bit-phase bins respectively; $f_S = 4.092$ MHz and $T_{coh} = 1$ s.

However, (43) can be rewritten as

$$R = \sum_{m=1}^{M} \widehat{d}_m R_m \tag{45}$$

where R_m is partial correlation value with representation in (5). With this approach, the acquisition stage can compute $R_1, R_2, ..., R_M$ then save these values for testing with all possible values of bit-phase. This approach in fact utilizes the coherent combination presented in (16). For this mechanism, the number of elementary steps is

$$[M(f_S \cdot T_{coh_1}) + M \cdot N_{bit-seq}] \cdot N_{cp} N_f = 4.192 \cdot 10^6 \cdot N_{cp} \cdot N_f \tag{46}$$

with M being the number of partial correlations obtained after 1-ms coherent integration time (T_{coh_1}). From (44) and (46), the computational complexity of the partial correlation approach has a reduction of approximately 2 orders of magnitude with respect to the conventional one.

5.4 Performance analyses

This section demonstrates the application of the test-bed for indoor signal acquisition. The required integration time for indoor signals is longer than for outdoor ones. The sky plot, see Fig. 10, has been generated by means of an auxiliary receiver with the antenna placed out of

the lab window, so to have and indication of the available GPS constellation. The distance between the antenna of the auxiliary receiver and the test indoor antenna is $\leq$ 10 m. The sky

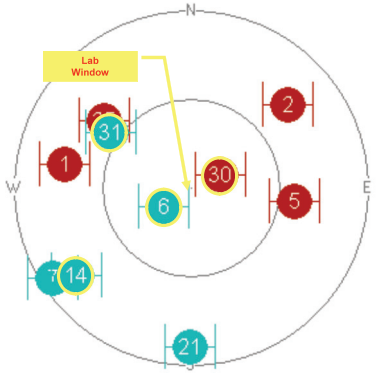

Fig. 10. Skyplot, indoor, Rb

plot relative to this case-study is depicted in Fig. 10. PRN6 and PRN30 are considered in this section. The assistance log is summarized in Table 4. Then the 3-step procedure in Section 5.2 is applied. Firstly, the strongest signal, which is PRN6 as seen in Table 4, is determined. After that, FFT-based acquisition is activated to search for PRN6 in the signal snapshot collected in indoor environment. Then the following procedure has been used to determine the assistance offsets and the corrected aiding data. For PRN6 the code phase from the assistance log is τ_6^a =120 chips. The preliminary fast acquisition on PRN6 estimated a code-phase τ_6^p = 1000.3 chips (Table 6). The code-phase offset is:

$$\delta\tau_6 = \tau_6^p - \tau_6^a = 880.3 \text{ chips} \tag{47}$$

As the signal snapshot is the same for the two PRNs, there are no time drifts to take into account. Therefore:

$$\tau_{30}^p = \delta\tau_{30} + \tau_{30}^a = \delta\tau_6 + \tau_{30}^a = 1060.3 \text{ chips} \tag{48}$$

It should be noted that because the full code length is 1023 chips, therefore, τ_{30}^p can also equal to 37.3 chips.

The same approach is used to compute the aiding value of Doppler frequency, $f_{D,30}^p = -0.6025$ kHz. Finally, after step 2, the aiding parameters are listed in Table 5.

The aiding parameters are used for acquiring the weaker satellite, PRN30, in indoor environment. The correlation results are shown in Fig. 11 and in Table 5, it can be noticed that the 3 dB rule still holds. In fact The signal of PRN 30 pass through the roof and the walls of the laboratory. Thus, it was good realizations of typical indoor signals and and it is detected by assisted coherent correlation.

6. Channel combination approach: Joint data/pilot acquisition strategies

In this section, the channel combination approach to improve the sensitivity of the acquisition is described. The considered signal is Galileo E1 Open Service signal. The current definition

PRN	Elevation (^{o})	C/N_0 (dB-Hz)	Code-phase (chips)	f_D (Hz)	r_D(Hz/s)
30	60	-	180	-635.0	-0.4
6	73	32.7	120	1067.5	-0.5

Table 4. Assistance log, indoor, Rb

PRN	Aiding source	$\tau^{(pred)}$ (chips)	$f_D^{(pred)}$ (kHz)
6	FFT	1000.3	1.1
30	Assistance server	1060.3 or 37.3	-0.6025

Table 5. Aiding data, indoor, Rb

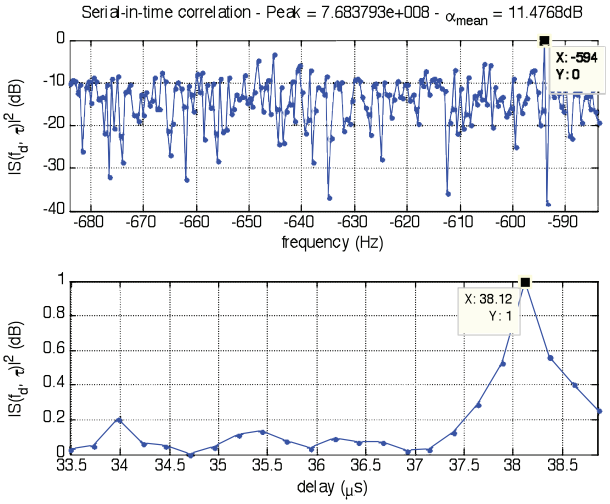

Fig. 11. Long coherent correlation, indoor, Rb, $T_{int} = 2000$ ms, PRN30

of the this signal (GalileoICD, 2008) includes data (B) and pilot (C) channels which are multiplexed by Coherent Adaptive Sub-carrier Modulation (CASM) (Dafesh et al., 1999). Each channels shares 50 % of the total transmitted power. To represent this signal, the common representation in (1) is changed to

$$r[n] = \frac{1}{\sqrt{2}}\sqrt{2C}\left(d[n+\tau]b[n+\tau] - c_{2nd}[n+\tau]c[n+\tau]\right)\cos\left(2\pi(f_{IF}+f_D)nT_S + \phi\right) + n_W[n] \tag{49}$$

$b[n]$, $c[n]$ are respectively the 4-ms primary PRN codes of the data (B) and pilot (C) channels modulated by BOC(1,1) scheme; $d[n]$ is the navigation data in the B channel; $c_{2nd}[n]$ is the secondary code, which together with $c[n]$ form a 100-ms tiered code for the C channel (GalileoICD, 2008). Basically, the conventional acquisition stage in Fig. 1 can perform on either B or C channels. This strategy is referred here as Single Channel (SC). However, SC also implies a waste of half of the real capability. Therefore, joint data/pilot acquisition strategies are introduced to utilize the full potential of the E1 OS signal (Mattos, 2005; Ta et al., 2010). In the followings, these strategies are described together with the performance evaluation.

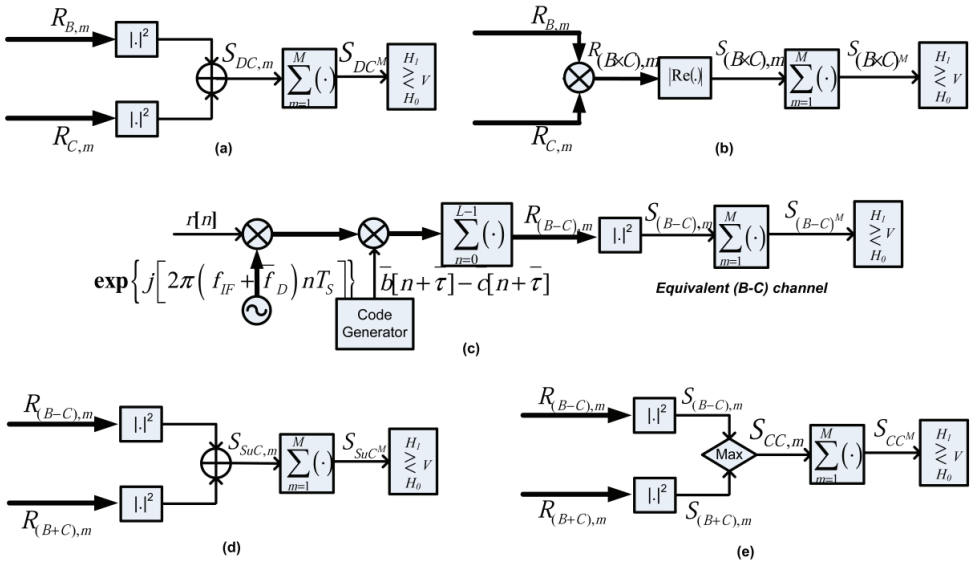

Fig. 12. Joint data/pilot acquisition architectures: (a) Dual Channels - DC; (b) (B×C); (c) Assisted (B-C); (d) Summing Combination - SuC; (e) Comparing Combination - CC

6.1 Joint data/pilot acquisition strategies

The correlation process performs on both channels to produce $R_{B,m}$ and $R_{C,m}$ (5). After that, these correlation values are combined as follows:

- Dual Channel (DC):

This strategy sums the square envelopes from the two channels, see Fig. 12(a). The decision variable is

$$S_{DC^K} = \sum_{m=1}^{M} \left(|R_B, m|^2 + |R_{C,m}|^2 \right) = \sum_{m=1}^{M} \left(|S_{B,m}|^2 + |S_{C,m}|^2 \right) \tag{50}$$

- (B×C):

In this strategy [see Fig. 12(b)], the decision variable is

$$S_{(B\times C)^M} = \sum_{i=1}^{M} |\{R_{B,i} \cdot R_{C,i}^*\}|^2 \tag{51}$$

This strategy can be seen as another realization of the conventional differential technique presented in Section 3.2.3. The correlator output in a channel is combined with the one from the other channel instead of the delayed copy of itself as in the conventional differential technique.

- Assisted (B-C):

The baseband E1 OS signal has the form $[d(t)b(t) - c_{2^{nd}}(t)c(t)]$. Due to the bi-polar nature of the data and secondary codes, the digital received baseband signal in each code period is always in one of the two representations

$$|b[n] - c[n]| \text{ or } |b[n] + c[n]| \tag{52}$$

This fact paves the way for a new strategy using one of the two equivalent codes $(\bar{b}[n] - \bar{c}[n])$ or $(\bar{b}[n] + \bar{c}[n])$ as the local code with the decision depending on the signal representation. Consequently, the two new equivalent channels (B-C) and (B+C) are defined. At a time instance, without the availability of an external-aiding source, because of the unknown navigation data bit, the acquisition stage cannot know the correct representation of the received signal, i.e. (B-C) or (B+C). In addition, the two new equivalent codes are orthogonal and still preserve the properties of the PRN codes (Ta et al., 2010). Therefore, if the chosen equivalent local code is incorrect, the correlation value in the equivalent channel might be null although the tentative parameters (i.e. PRN number, Doppler and code delay) are correct, because of the unknown data bit sign. Hence, the availability of an external-aiding source is crucial.

Without loss of generality, let us assume that the external-aiding source assures the signal structure is $(b[n] - c[n])$, therefore, the (B-C) strategy is applied, see Fig. 12(c). The decision variable of the assisted (B-C) is

$$S_{(B-C)^M} \triangleq \left| R_{(B-C)^M} \right|^2 = \left| \sum_{m=1}^{M} R_{(B-C),m} \right|^2 \tag{53}$$

Note that: for this external-aiding scenario, the coherent combination is used.

However, in one full primary code period, the signal can be only in one of the two representations in (52), it is worth to test both the strategies [i.e. (B-C) and (B+C)] and combine their results. This leads to two new strategies so-called Summing Combination and Comparing Combination.

- Summing Combination (SuC):

In this strategy (see Fig. 12(d)), the (B-C) and (B+C) strategies are simultaneously performed. The square envelope outputs are summed up to form the new decision variable

$$S_{SuC} = S_{(B-C)} + S_{(B+C)} = |R_{(B-C)}|^2 + |R_{(B-C)}|^2 = 2(|R_B|^2 + |R_C|^2) \tag{54}$$

In this way, the overall decision variable is no longer affected by the unknown polarity of the data and secondary codes of the received signal. However, multiplying the decision variable by any coefficient does not affect the ultimate performance of a strategy because the signal and the noise powers are increased by the same rate. Therefore, the SuC strategy shares the performance with the DC strategy. For this reason, in the following sections, only the DC strategy is considered.

- Comparing Combination (CC):

This strategy (see Fig. 12(e)) uses a comparator instead of the adder as in the SuC strategy to combine the square envelope outputs of the two equivalent channels. The larger value is

chosen to be the decision variable

$$S_{CC^M} = \sum_{m=1}^{M} \max\left\{S_{(B-C),m}, S_{(B+C),m}\right\} \tag{55}$$

The analytical expressions of the performance parameters of these strategies are presented in (Ta et al., 2010).

6.2 Performance analyses

Fig. 13 clearly shows the improvement of the joint data/pilot strategies over the conventional SC. The benchmark values $P_{fa} = 10^{-3}$ and $P_d = 0.9$ for the hypothesis testing in GNSS receivers are used to quantitatively estimate the improvement. When only one full code

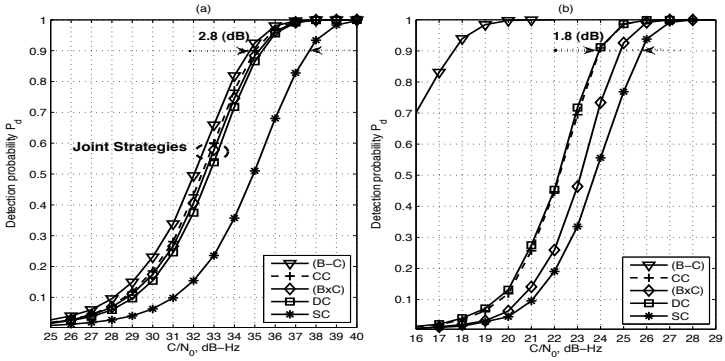

Fig. 13. Detection probability of all the strategies vs. C/N_0 values when $P_{fa} = 10^{-3}$: (a) $M = 1$; (b) $M = 50$

period is considered (i.e. $M = 1$), as shown in Fig. 13(a), the joint data/pilot strategies holds the sensitivity enhancement ~ 3 dB over the conventional SC. Among the joint strategies, the assisted (B-C) outperforms the others, because the assistance data always guarantees the local generated signal matching the most to the received one. As for the other stand-alone joint strategies, the difference in P_d is small, but one still can realize that CC is the best one.

When $K = 50$, the assisted (B-C) is far better than the others, because the coherent combination applied in this strategy brings more performance improvement than the other strategies using the non-coherent technique suffering from the squaring loss phenomenon. This loss also reduces the enhancement (from 2.8 dB to 1.8) dB) of the stand-alone joint strategies with respect to the SC, see Fig. 13(b). Among the stand-alone joint strategies, in this scenario, DC takes the position of CC to be the best. While (B$\times$C) degrades significantly, because unlike $K = 1$, for $K > 1$, to secure the accumulation, the absolute values of the differential operation's outputs are used in the non-coherent combination. This fact makes the averaging not thorough.

Fig. 14 shows the $\overline{T}_A$ values of all the strategies. It should be note that $\overline{T}_A$ simultaneously consider the influences of both the computational complexity and the sensitivity of a strategy.

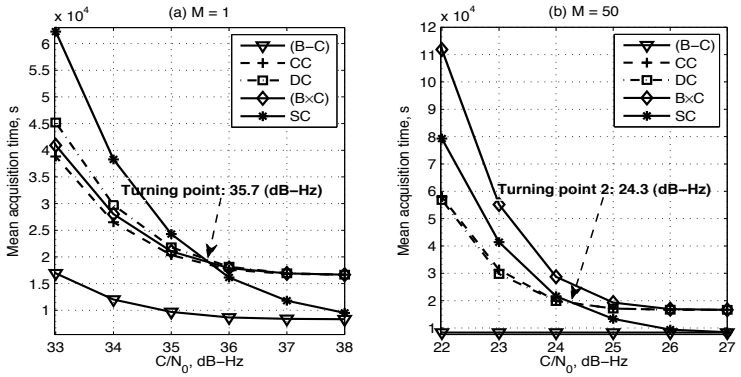

Fig. 14. Mean acquisition time $\overline{T}_A$ vs. C/N_0 values when $P_{fa} = 10^{-3}$: (a) $M = 1$; (b) $M = 50$

For all C/N_0 and K values, (B-C) results in the smallest $\overline{T}_A$, because of its high sensitivity (i.e. detection capability) and also moderate complexity (only one correlator required, but assistance is needed). For $K = 1$ and 33 (dB-Hz) $\leq C/N_0 <$ 36 (dB-Hz), due to the significant sensitivity improvement of the DC, (B×C), and CC strategies with respect to the SC strategy, their $\overline{T}_A$ values are smaller than that of the SC strategy, see Fig. 14(a). However, for $C/N_0 \geq$ 35.7 (dB-Hz), the sensitivity improvement of the SC strategy is sufficient to reduce its $\overline{T}_A$ to be lower than that of the stand-alone joint strategies. For $K = 50$, due to the sensitivity improvement of all the strategies, the turning point appears earlier at $C/N_0 = 24.3$ (dB-Hz). see Fig. 14(b).

7. Conclusions

This Chapter focused on high sensitivity signal acquisition problems. Throughout the chapter, some challenges to HS signal acquisition such as unknown data transitions, Doppler effects on carrier frequency and PRN code rate, local oscillator instability as well as sensitivity-complexity trade-off were discussed in details in order to define the requirements of HS acquisition strategies suitable for different operational scenarios. Then three HS acquisition approaches, namely stand-alone, external-aiding and channel combining, have been introduced. Finally, the applications of these approaches to specific GNSS signals are demonstrated for readers' better understanding.

8. References

3GPP (2008a). Radio resource control (RRC) - release 7, *Organizational Partners* .

3GPP (2008b). Radio resource LCS protocol (RRLP) - release 7, *Organizational Partners* .

Audoin, C. & Guinot, B. (2001). *The Measurements of Time - Time, Frequency and the Atomic Clock*, Cambridge University Press.

Betz, J. W. (2001). Binary Offset Carrier Modulations For Radionavigation, *Journal of Navigation* 48: 227–246.

Chansarkar, M. & Garin, L. (2000). Acquisition of GPS Signals at Very Low Signal to Noise Ratio, *Proceedings of the 2000 National Technical Meeting of the Institute of Navigation (ION NTM 2000), Anaheim, CA, USA*, pp. 731–737.

Choi, I. H., Park, S. H., Cho, D. J., Yun, S. J., Kim, Y. B. & Lee, S. J. (2002). A Novel Weak Signal Acquisition Scheme for Assisted GPS, *Proceedings of the ION GPS 2002, Portland, OR, USA*, pp. 177–183.

Corazza, G. E. & Pedone, R. (2007). Generalized and Average Likelihood Ratio Testing for Post Detection Integration, *IEEE Transactions on Communications* 55: 2159–2171.

Dafesh, P. A., Nguyen, T. M. & Lazar, S. (January 1999). Coherent Adaptive Subcarrier Modulation (CASM) For GPS Modernization, *Proceedings of ION NTM 1999, San Diego, CA, USA*, pp. 649–660.

Park, S. H., Choi, I. H., Lee S. J., & Kim, Y. B. (2002). A Novel GPS Initial Synchronization Scheme using Decomposed Differential Matched Filter, *Proceedings of ION NTM 2002, San Diego, CA, USA*, pp. 246–253.

Datum8040 (1998). DATUM 8040 Rubidium frequency standard - Technical specifications.

Djuknic, G. M. & Richton, R. E. (2001). Geolocation and assisted GPS, *IEEE Computer* 34(2): 123–125.

Dodds, D. & Moher, M. (1995). Spread Spectrum Synchronization for a LEO Personal Communications Satellite System, *Canadian Conference on Electrical and Computer Engineering 1995 (CCECE '95), Montreal, PQ, Canada*, pp. 20–23.

Dovis, F., Lesca, R., Boiero, G. & Ghinamo, G. (2010). A Test-bed Implementation of An Acquisition System for Indoor Positioning, *GPS Solutions* 14(3): 241–253.

Elders-Boll, H. & Dettmar, U. (2004). Efficient Differentially Coherent Code/Doppler Acquisition of Weak GPS Signals, *Proceedings of the IEEE International Symposium on Spread Spectrum Techniques and Applications (ISSSTA 2004), Sydney, Australia*, pp. 731–735.

GalileoICD (2008). Galileo Open Service, Signal In Space Interface Control Document Draft 1, *Technical report*, European GNSS Supervisory Authority / European Space Agency.

Gernot, C., Keefe, K. O. & Lachapelle, G. (2008). Comparison Of L1 C/A L2C Combined Acquisition Techniques, *Proceedings of ENC-GNSS 2008, Toulouse, France*.

GPS-IS (2006). Navstar GPS Interface Specification IS-GPS-200 revision D, *Technical report*, Navstar GPS Joint Program Office.

Holmes, J. K. (ed.) (2007). *Spread Spectrum Systems for GNSS and Wireless Communications*, Artech House.

HP (1990). 325B Synthesizer/Function Generator Service Manuald, *Agilent Technologies* .

Kaplan, E. D. (ed.) (2005). *Understanding GPS: Principles and Applications*, 2nd edn, Artech House.

Kreiszig, E. (1999). *Advanced Engineering Mathematics*, John Wiley and Sons.

Mattos, P. G. (2005). Acquisition of the Galileo OAS L1b/c signal for the mass-market receiver, *Proceedings of ION GNSS 2005, Long Beach, CA, USA*, pp. 1143–1152.

Misra, P. & Enge, P. (2006). *Global Positioning System: Signals, Measurements, and Performance*, 2nd edn, Ganga-Jamuna Press.

Mulassano, P. & Dovis, F. (2010). *Assisted Global Navigation Satellite Systems: An Enabling Technology for High Demanding Location-Based Services*, CRC Press.

OMA (2007). Secure user plane for location (SUPL), *Open Mobile Alliance* .

Persson, B., Dodds, D. & Bolton, R. (2001). A Segmented Matched Filter for CDMA Code Synchronization in Systems with Doppler Frequency Offset, *in* 1 (ed.), *Proceedings of IEEE Globecom '01, San Antonio, Texas, USA*, pp. 648–653.

Schmid, A. & Neubauer, A. (2004). Perfomance Evaluation of Differential Correlation for Single Shot Measurement Positioning, *Proceedings of ION GNSS 2004, Long Beach, CA, USA*, pp. 1998–2009.

Shanmugam, S. K., Nielsen, J. & Lachapelle, G. (2007). Enhanced Differential Detection Scheme for Weak GPS Signal Acquisition, *Proceedings of ION GNSS 2007, Fort Worth, TX, USA*, pp. 2499–2509.

Shanmugam, S. K., Watson, R., Nielsen, J. & Lachapelle, G. (2005). Differential Signal Processing Schemes for Enhanced GPS Acquisition, *Proceedings of ION GNSS 2005, Long Beach, CA, USA*, pp. 212–222.

Ta, T. H. (2010). *"Acquisition Architecture for Modern GNSS Signals"*, PhD thesis, Polytechnique University of Turin, Italy.

Ta, T. H., Dovis, F., Lesca, R. & Margaria, D. (2008). Comparison of Joint Data/Pilot High-Sensitivity Acquisition Strategies for Indoor Galileo E1 Signal, *Proceedings of ENC-GNSS 2008, Toulouse, France*.

Ta, T. H., Dovis, F., Margaria, D. & Presti, L. L. (2010). Comparative Study on Joint Data/Pilot Strategies for High Sensitivity Galileo E1 Open Service Signal Acquisition, *IET Radar, Sonar and Navigation* 4, Issue 6: 764–779.

Ta, T. H., Qaisar, S. U., Dempster, A. & Dovis, F. (2012). Partial Differential Post Correlation Processing for GPS L2C Signal Acquisition, *IEEE Transactions on Aerospace and Electronic Systems* 48, Issue 2.

Tsui, J. B.-Y. (2005). *Fundamentals of Global Positioning System Receivers: a Software Approach*, 2nd edn, Wiley-Interscience.

Vig, J. (2005). Quartz crystal resonators and oscillators for frequency control and timing applications - a tutorial, *IEEE Ultrasonics, Ferroelectrics, and Frequency* .

Wilde, W. D., Sleewaegen, J.-M., Simsky, A., Vandewiele, C., Peeters, E., Grauwen, J. & Boon, F. (2006). New Fast Signal Acquisition Unit for GPS/Galileo Receivers, *Proceedings of European Navigation Conference ENC-GNSS 2006*.

Yu, W., Zheng, B., Watson, R. & Lachapelle, G. (2007). Differential combining for acquiring weak GPS signals, *Signal Processing* 87(5): 824–840.

Zarrabizadeh, M. H. & Sousa, E. S. (1997). A Differentially Coherent PN Code Acquisition Receiver for CDMA Systems, *IEEE Transactions on Communications* 45(11): 1456–1465.